JOURNAL OF MATERIALS SCIENCE **38** (2003) 1255–1267

Influence of oxides on porosity formation in Sr-treated Al-Si casting alloys

L. LIU, A. M. SAMUEL, F. H. SAMUEL
Département des Sciences appliquées, Université du Québec à Chicoutimi, Chicoutimi (Québec), Canada G7H 2B1
E-mail: fhsamuel@uqac.ca

H. W. DOTY
Materials Engineering, GM Powertrain Group, Metal Casting Technology, Inc., Milford, NH 03055, USA

S. VALTIERRA
Research and Development, Corporativo Nemak, S.A. de C.V., P.O. Box 100 Bosques del Valle, Garza Garcia, N.L. 66221, Mexico

The strength and quality of an Al-Si alloy casting are determined by its microstructure and the amount of porosity present in the casting. Modification is one of the processes used to improve the microstructural quality, where the addition of a modifying agent alters the shape of the eutectic Si from an acicular to a fibrous form that is extremely beneficial to the mechanical properties. Among various modifiers, strontium has been used extensively, as it is easier to handle and more resistant to fading. However, its addition is also associated with porosity formation in these alloys. The porosity formed in Sr-modified castings has been variously related to an increase in the hydrogen level of the melt, feedability problems in the mushy zone during solidification, and changes in the mode of eutectic nucleation—from near the α-Al dendrites in the Sr-free alloy, to within the eutectic liquid itself in the Sr-containing alloy. The present study was carried out to determine the influence of oxides on the porosity characteristics observed in Al-Si alloys containing strontium. A series of experimental and industrial alloys viz., Al-7%Si, Al-12%Si, 319 and 356 were selected, to cover a variety of alloy freezing ranges. The techniques of thermal analysis, optical microscopy, and SEM/EDX and EPMA analyses were employed to obtain the results presented here. It is seen how the presence of oxides (Sr and Al) is responsible for the porosity formation observed in Al-Si alloys, and that the difference in porosity characteristics with the addition of Sr depends on the amount of Sr oxides present in the solidified structure. The presence of aluminum oxide films leads to the formation of large pores that are often linked together. Both aluminum and strontium oxides are favorable sites for the nucleation of other microconstituents.

1. Introduction

The strength and quality of an Al-Si alloy casting are determined by the quality of its microstructure, viz., the fineness of the structure, the shapes and morphologies of the microconstituents present therein, as well as the amount of porosity produced in the casting. Normally, the microstructure is controlled through the processes of grain refinement and modification, using small additions of Al-Ti-B and Al-Sr master alloys, respectively. Whereas grain refinement primarily reduces the grain size, modification—using elements such as Na, Sr, Sb, or even rare earths—alters the shape of the eutectic Si from its usual acicular brittle from to a fibrous form (in the case of Na and Sr) that is extremely beneficial to the mechanical properties, particularly the ductility. Among the various modifiers in use, strontium has, by far, been employed most extensively. Although easier to handle than either Na or the toxic Sb, and more resistant to fading (i.e., losing its modifying effect after a certain amount of time), Sr addition is also associated with porosity formation in these alloys.

A tremendous amount of work has been carried out to study Sr-related porosity, one of the earliest perhaps being that of Argo and Gruzleski [1] on porosity in Sr-modified A356 aluminum alloy castings, in which the authors distinguished between the fundamental differences in microshrinkage and microporosity formation in unmodified and Sr-modified hypoeutectic Al-Si alloys, using A356 alloy as an example. Lee and Sridhar [2] and Fuoco *et al*. [3] have commented that the effect of strontium on porosity formation is not well understood, even if the observations that a higher tendency

for microporosity and an increase in percentage porosity in Sr-modified alloys are generally agreed upon in the literature.

McDonald *et al*. [4] have pointed out that despite all the research carried out on Sr-related porosity, only a few workers have investigated a range of Sr concentrations. What these studies do reveal, however, is that a vast difference in porosity characteristics is observed between Sr-free and Sr-containing castings. The Sr concentration is apparently not a critical factor in this regard, as such changes are even observed in alloys containing very low levels of Sr.

As the formation of gas porosity is directly related to the amount of dissolved hydrogen in the melt, the increase in porosity level with Sr addition was naturally assumed to be related to an increase in the hydrogen level of the melt. To this end, Denton and Spittle [5] reported that Sr-containing melts had a higher rate of gas absorption from their surroundings, attributed to the possibility of a more permeable oxide layer. Other studies [6] showed that Sr additions do not normally introduce hydrogen into the melt, while yet others reported a decrease in the hydrogen content, e.g., Shahini [7], who related an increase in the density of reduced pressure test samples to a decrease in the hydrogen content.

These contradictions led researchers to focus on the problem of feedability in the mushy zone during solidification. As Sr results in depressing the eutectic Si temperature, the mushy zone (α-Al dendrite solidification) region of the alloy is increased, and the increase in porosity levels observed with Sr addition is thus attributed to the latter. However, although this is true to a certain extent, the corresponding increase in freezing range does not satisfactorily explain the much higher increase in porosity levels observed in Sr-modified alloys [3].

Further extending the feedability-related point of view, it has also been pointed out that one should look to the Al-Si eutectic region of solidification to explain the differences in porosity observed when Sr is added to Al-Si melts [5, 8, 9]. Given that the eutectic constitutes almost half the microstructure of Al-Si alloys, it would be expected that the Sr-modified eutectic structure would exert some sort of influence on porosity formation. In this connection, Dahle *et al*. [10], who observed an orientation relationship between the α-Al dendrites and eutectic Si in unmodified hypoeutectic Al-Si alloys, and a lack of it in the (200 ppm) Sr-modified alloys (using electron micro-diffraction techniques), have suggested that this represents a change in the mode of eutectic nucleation—from that occurring near the α-Al dendrites in the Sr-free alloy, to that taking place within the eutectic liquid itself in the Sr-containing alloy. The mode in operation controls the distribution of the remaining liquid in the last stages of solidification when feeding becomes extremely difficult. This distribution, in turn, will define the connectivity of the feeding channels, and thus determine the resultant porosity profile in the solid casting.

In reviewing the literature, it is interesting to note that a number of small, but important, details in regard to Sr-related porosity are mentioned in passing, but the possibility of considering oxides as being responsible for these observations has not been taken too much into account, possibly due to the difficulties associated with the measurement of oxides, from both qualitative and quantitative points of view. In fact, Iwahori *et al*. [11, 12] appear to be the earliest researchers to mention an oxide-related connection: they reported that the hydrogen level in Sr-modified melts is not lowered by vacuum degassing, and attributed this to the fact that hydrogen absorbed into the oxide in the melt is more strongly fixed in the oxide by the addition of strontium to the melt (the oxides being considered as inclusions in the melt). According to them, in order to produce porosity-free castings, it is necessary to eliminate oxide inclusions from the melt before it is modified with Sr or degassed.

In this regard, Jacob *et al*. [13] observed that Sr additions to Al-Si alloys produced thicker but non-homogeneous surface oxide layers, which exhibited SrO regions up to 500 μm long. Lee and Sridhar [2], who carried out *in situ* observations of pore nucleation and growth in Sr-, and ($Sr + TiB_2$)-treated Al-Si alloy melts using an X-ray temperature gradient stage (XTGS) technique, alluded to this point in their work, but could not, however, detect such oxides with their XTGS apparatus. In another context, Cao and Campbell [14] have also pointed out the influence of oxide films folded into the melt during pouring as being conducive to porosity formation.

It is the aim of the present study to show how the presence of oxides (Sr and Al) in the molten metal is the factor that mainly influences the porosity observed in Sr-containing Al-Si alloys. A series of experimental and industrial Al-Si casting alloys were selected for study, from simple experimental "binary" alloys such as Al-7%Si and Al-12%Si, to industrial 319 and 356 alloys, to cover a variety of alloy freezing ranges. As mentioned previously, it will be shown how the difference in porosity characteristics does not depend on the actual Sr level in the alloy, but on the presence of Sr and/or Al oxides in the molten metal and, consequently, in the solidified structure. The techniques of thermal analysis, optical microscopy, and SEM/EDX and EPMA analyses were employed to obtain the results that have been presented here.

It should be mentioned at the outset, that the "binary" alloys in the present study are termed "binary" only in the sense that Al and Si are their main constituents, as against other alloying elements that are present in addition in the 356 and 319 alloys. As the chemical analyses listed in Table I show, these binary alloys also contain a certain amount of impurities, in spite of the fact that they were prepared from relatively pure (99.95%) Al and Si.

2. Experimental

Table I lists the chemical compositions of the various alloys that were used in the present work and their respective alloy codes. The alloys were cut into smaller pieces, cleaned, dried and melted in a 40 kg-capacity SiC crucible. The melting temperature was kept at $725^\circ \pm 5^\circ$C.

TABLE I Chemical composition (wt%) of alloys used

Alloy	Code	Si	Fe	Cu	Mg	Mn	Cr	Ti	Sr	Al
Experimental										
Al-7% Si	A7S	6.74	0.1599	0.2825	0.0228	0.0316	0.0051	0.0246	0.0018	92.7
Al-7%Si + Sr	A7SS	6.71	0.1891	0.3656	0.0340	0.0331	0.0064	0.0274	0.0114	92.6
Al-12%Si	Al2S	11.76	0.1451	0.1144	0.0119	0.0072	0.0012	0.0413	0.0010	87.9
Al-12%Si + Sr	Al2SS	11.76	0.1451	0.1144	0.0119	0.0072	0.0012	0.0413	0.0245	87.8
Industrial										
319	A7SC	6.24	0.1084	3.683	0.0496	<0.0005	<0.0005	0.1332	0.0001	89.7
319 + Sr	A7SCS	5.81	0.1145	3.584	0.0552	<0.0005	<0.0005	0.1466	0.0115	90.2
356	A7SM	6.50	0.1211	0.0470	0.3194	0.0008	0.0008	0.1110	0.0001	92.8
356 + Sr	A7SMS	6.47	0.1332	0.0398	0.3283	0.0020	0.0020	0.1164	0.0070	92.8

The melts were degassed with dry argon for ~30 min, by means of a graphite rotary impeller (200 rpm; humidity of surroundings <15%). A 5 cm wide, 25 cm long plate made of refractory material, placed inside the crucible at an angle of ~35 degrees with the crucible wall acted as a baffle during the melting and degassing process, to avoid vortex formation. In those cases when the melts were modified with Sr, the required amount of Sr was added to the melt using Al-10% Sr master alloy, before the degassing was carried out. All melts were grain refined using Al-5%Ti-1%B master alloy (boron concentration was about 40 ppm).

In the case of the experimental alloys, the alloys were first prepared by melting commercially pure aluminum (purity ≅ 99.5%) at the same temperature, then adding pure silicon in the required amounts by means of a perforated graphite bell, to obtain the Al-7%Si and Al-12%Si alloys. The alloy melts were poured into ingot molds, and the solidified ingots were used as described above. Samplings for chemical analysis were also taken simultaneously for each pouring. Hydrogen content was monitored using an Alscan apparatus. In most cases, the hydrogen concentration was approximately 0.08 ml/100 g Al.

About 1 kg of the degassed melt was transferred by means of a ladle into a 1 kg-capacity SiC crucible (length/diameter ratio: 130 cm:85 cm) that was preheated at 750°C in a small electric resistance furnace. The transfer procedure was carried out with extreme caution to minimize turbulence, and took about 10 min. During the transfer, the SiC crucible was initially tilted at ~35 degrees, then raised slowly while the liquid metal was poured into it, till it was in an upright position at the end of the filling. When the melt temperature in the crucible stabilized at 725°C, the melt was poured into a preheated (600°C) cylindrical graphite mold (10 cm length, 6 cm diameter), as shown in Fig. 1. Again, for each pouring (into the graphite mold), a sampling for chemical analysis was also done simultaneously (the spectrometric analyses were carried out at GMPT, New Hampshire facilities).

For metallographic examination, samples (25 mm × 25 mm) were sectioned from the graphite mold castings. The microstructures were analyzed using a Leco 2001 image analyzer in conjunction with an Olympus optical microscope. Phase identifications were carried out using electron probe microanalysis (EPMA), and energy dispersive X-ray (EDX) analysis, employing a Jeol WD/ED combined microanalyzer operating at 20 kV and 30 nA (electron beam size of ~1 μm).

3. Results and discussion

In this section, examples of the different types of pores observed in these alloys will be discussed. Based upon scanning electron microscopy (SEM), energy dispersive X-ray (EDX) spectroscopy, and electron probe microanalysis (EPMA) results, it will be shown how, in each case, these pores are associated with the presence of strontium oxide films or particles, within or in the vicinity of the pores. Table II shows that, compared to the porosity values obtained from well-degassed 319 alloy melt samples (hydrogen level ≈ 0.1 mL/100 g Al, as measured by the Alscan machine), the porosity levels displayed by samples taken from 319 alloys melts that were deliberately gassed (hydrogen level ≈ 0.25 mL/100 g Al) were comparatively much higher.

It is well known that micropores can be rounded or irregular; the former are those mostly associated with hydrogen gas, while the latter—also classified as "interdendritic"—arise due to the effects of shrinkage [15]. In their studies of gas porosity and metal cleanliness in 356 and 319 casting alloys, Laslaz and Laty [16] remarked that gas porosity after solidification depends not only on the hydrogen content of the melt, but also on metal cleanliness—in terms of the oxides present in the melt. The oxides were incorporated into the melt either by stirring or by adding chips cut from the same ingots used for melting. Furthermore, they proposed that their observations of round pores being associated with a strongly oxidized melt, and elongated pores with a cleaner melt, supported the hypothesis that pores nucleate on oxide inclusions. They also suggested

TABLE II Percentage porosity observed in Al-7%Si and 319 alloys

Alloy	Hydrogen level (mL/100 g)	Alloy code[a]	Percentage Porosity (%) No Sr	Alloy code[a]	250 ppm Sr
Al-7%Si	0.1	A7S (351s)	0.36	A7SS (360s)	0.86
319	0.1	A7SC (517s)	2.2	A7SCS (529s)	2.3
	0.25[b]		2.86[b]		3.4[b]

[a]Total solidification times (s) given in parentheses below the alloy codes.
[b]Gassed melt.

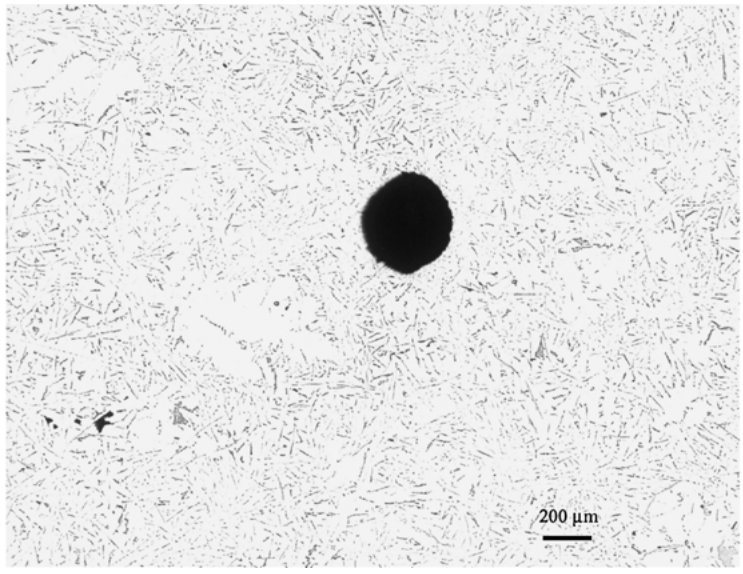

(a)

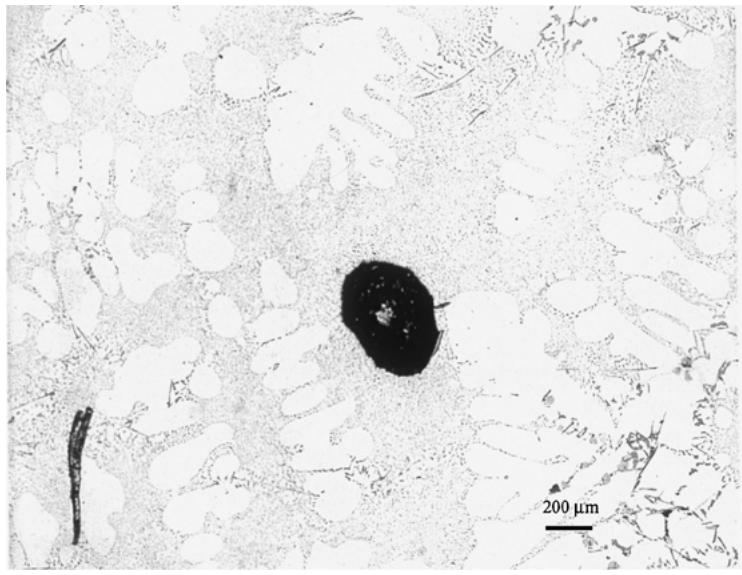

(b)

Figure 1 Optical micrographs showing pore types observed in: (a) unmodified, (b) Sr-modified Al-12%Si alloy.

the possibility that Sr increases the ability of the oxides to nucleate pores.

3.1. Role of strontium oxide

Fig. 1a shows an example of a rounded pore observed in the Al-12%Si alloy, surrounded mostly by eutectic Si regions. As can be seen, nothing is seen within the pore. As Fuoco *et al*. [15] have observed, pores will tend to have a rounded morphology if they are surrounded by eutectic Si cells/regions—as in the case of high silicon (>10%) alloys, rather than being impinged upon by dendrite arms that would alter their initial round shape. This is what is observed in Fig. 1a, in the unmodified alloy, viz., even in the absence of Sr. Thus, it is not so much the fact that rounded pores are observed in modified alloys, as that they are observed surrounded by eutectic Si regions. Fang and Granger [17] are also of the opinion that the rounded pore morphology in A356 alloy is due to the high eutectic volume fraction associated with the alloy.

The optical micrograph of Fig. 1b also shows a rounded pore, this time in the modified Al-12%Si alloy (250 ppm Sr). Again, the pore is seen surrounded by eutectic Si regions. However, in this case, the presence of fine particles can be noted inside the pore. An SEM micrograph of such a pore, Fig. 2a, provided greater details of the contents of the pore: several white particles could be observed within its interior (note also the presence of β-Al_5FeSi platelet fragments (arrowed)). Fig. 2b shows the nature of these particles at high magnification. These particles were identified as being AlSrO, as confirmed by the composite EDX and oxygen scans shown in Fig. 2c. It should be noted that the Kα line of Si and the Lα line of Sr have closely similar energies, thus resulting in the thick peak oberved in the EDX spectrum (see arrows). The exact stoichiometry of these particles could not be determined, however, due to the depth of the pore. Fig. 2d, taken at a much higher magnification, shows an example of the microporosity (arrowed) associated with the presence of these AlSrO particles.

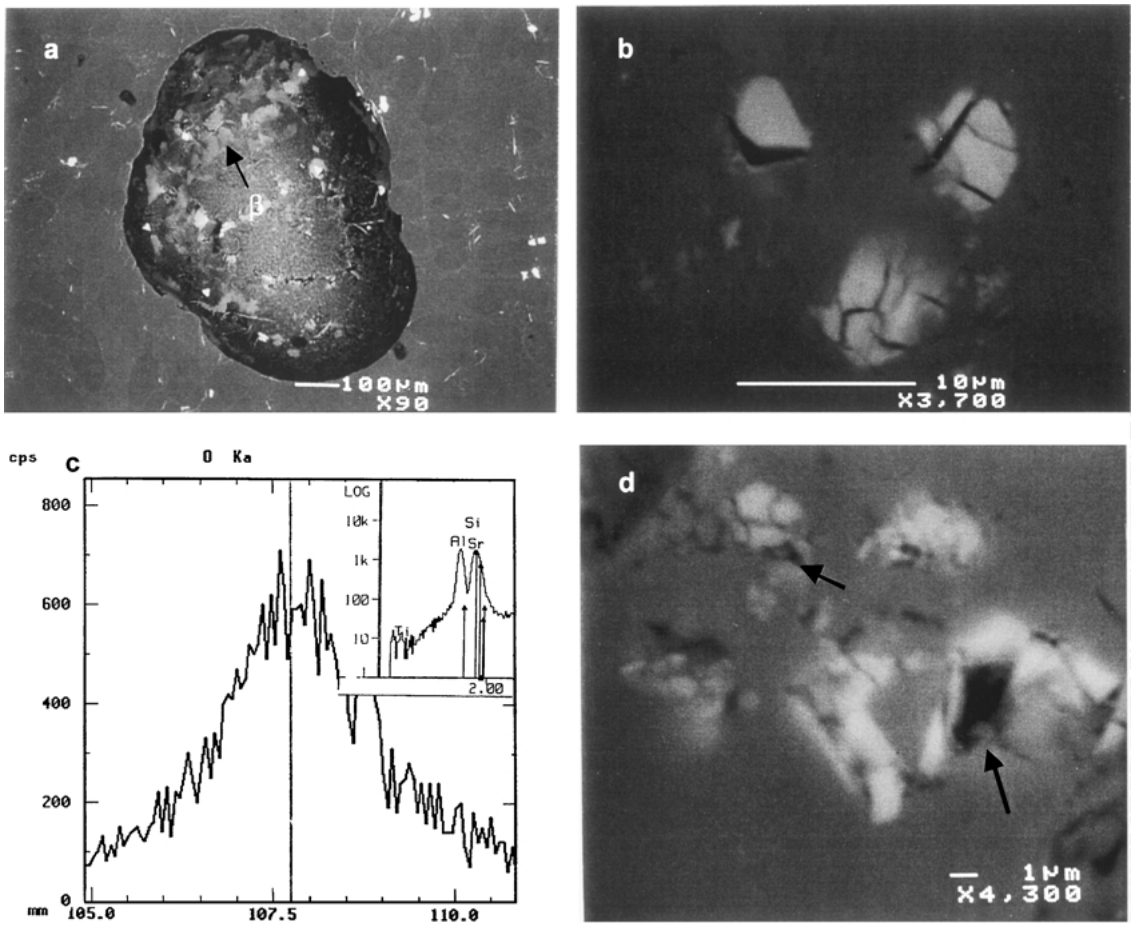

Figure 2 (a) SEM micrograph showing white particles inside a pore in Sr-modified Al-12%Si alloy, (b) high magnification SEM showing AlSrO particles, (c) composite of oxygen scan and EDX spectrum (inset) corresponding to AlSrO particles, (d) high magnification SEM showing microporosity associated with AlSrO particles (arrowed).

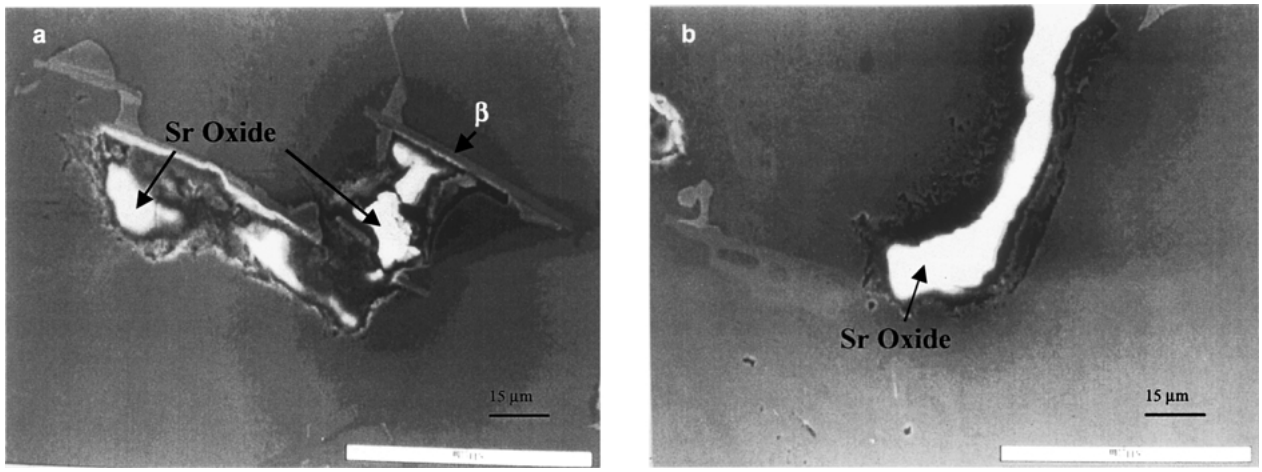

Figure 3 SEM micrographs showing irregular shrinkage type pores in Sr-modified 319 alloy. Note the presence of Sr oxides within, and β-Al_5FeSi platelets along the edges of the pore.

Fig. 3a demonstrates a shrinkage-type pore, with an irregular morphology in the Sr-modified 319 alloy. Two features are noted: (a) the presence of β-Al_5FeSi platelets along the edges of the pore, and (b) the presence of strontium oxide films and/or particles inside the pore. In a previous study (Samuel *et al*. [18]) it was shown that the β-Al_5FeSi phase could be nucleated on Al_2O_3 or MgO particles existing in the melt. From Fig. 3a, it could also be expected that the SrO films would also act as nucleation sites for the β-phase (arrowed). Another example of a thick strontium oxide film within a shrinkage cavity in the same alloy sample is shown in Fig. 3b. Cao and Campbell [14] have also reported that the wetted sides of double oxide films appear to act as nucleation sites for iron intermetallics.

In this connection, it ought to be mentioned that in another study [19] by our group, in which the reliability of the Qualiflash filtration technique in the measurement of oxide films in A356 and A390 aluminum foundry alloys was assessed, it was also observed how

the aluminum oxides were found associated with various microconstituents such as primary Si, MgO and TiB_2 particles.

In a recent study, Huang *et al*. [20] investigated the types of oxide films that can occur in pure Al, Al-Si and Al-Si-Mg alloys. They found that the polished specimens of these alloys exhibit "shining" spots that are in reality oxide films or particles, and suggested the use of an ultrasonic vibration technique that could assist (to a certain extent) in identifying these oxides. In the case of the Al-Si-Mg alloys, spinel was also observed to form. It is worth noting here that the strontium oxide regions

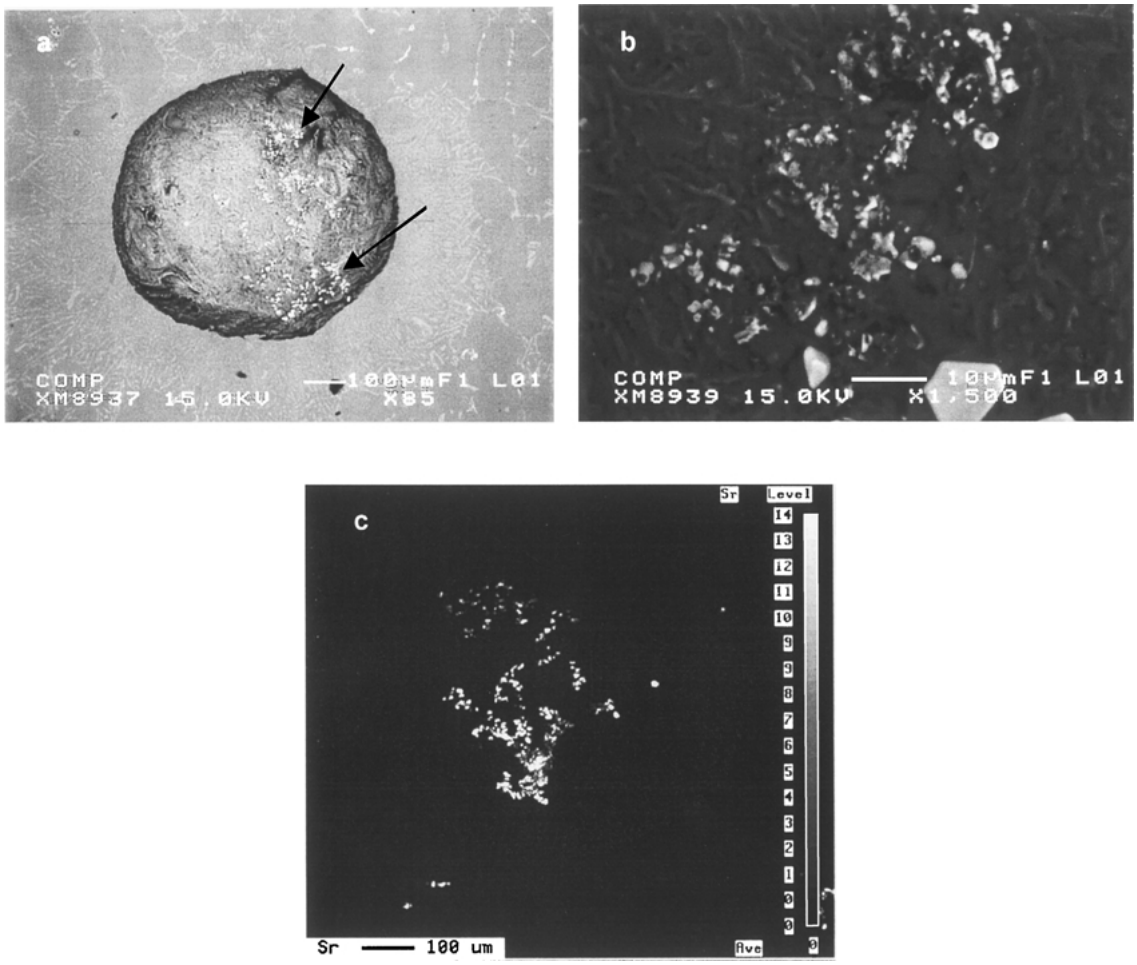

Figure 4 SEM micrographs obtained from an RPT sample of Sr-modified 356 alloy showing: (a) a pore with fine white AlSrO particles (arrows) at bottom, (b) size and distribution of AlSrO particles, (c) Sr image of AlSrO particles in (a).

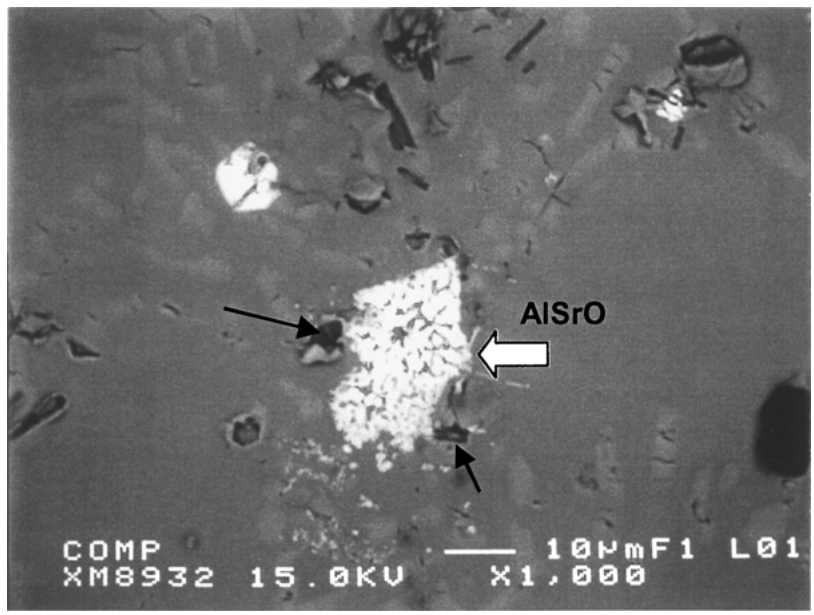

Figure 5 SEM micrograph of a Prefil test sample obtained from the same Sr-modified 356 alloy melt (Fig. 4), showing microporosity (black arrows) associated with strontium oxide clusters (white arrow).

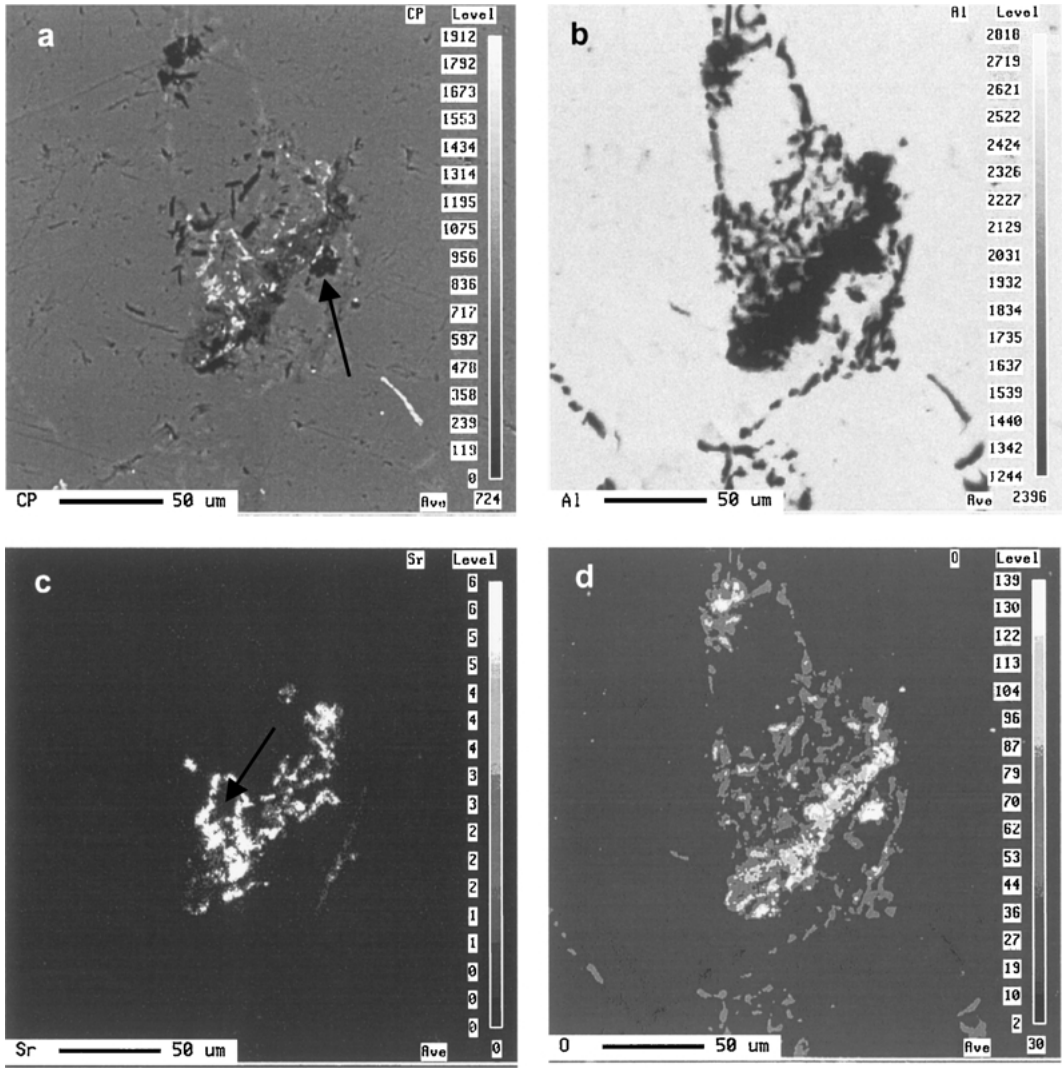

Figure 6 EPMA analysis of the Prefil test sample of Sr-modified 356 alloy showing: (a) the backscattered image of AlSrO films and associated microporosity, and (b) the Al-, (c) Sr-, (d) O images obtained from the AlSrO films.

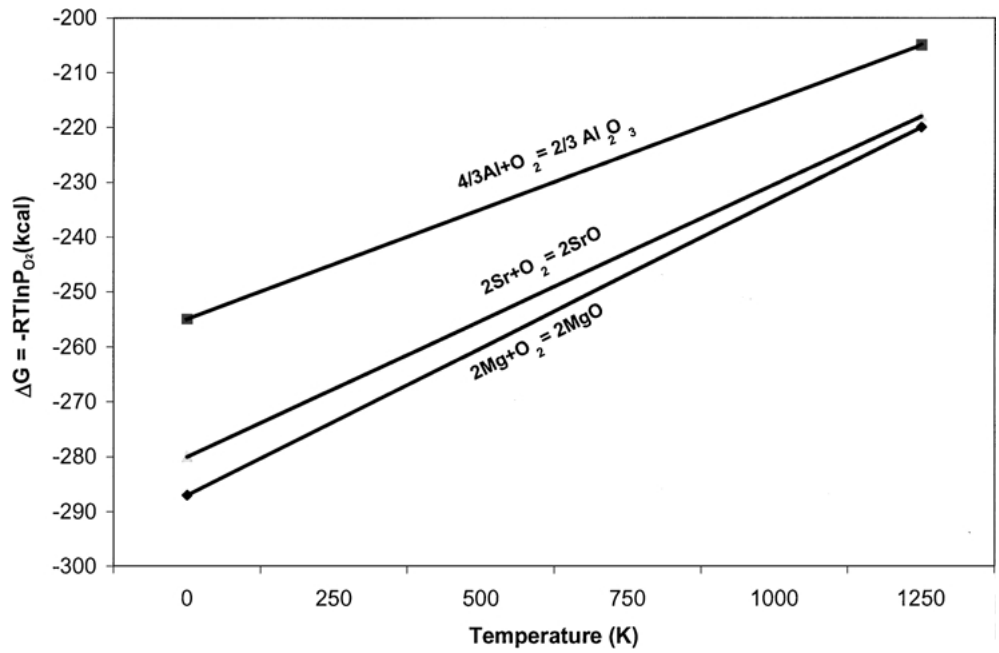

Figure 7 Free energies of formation versus temperature for Al, Sr and Mg oxides.

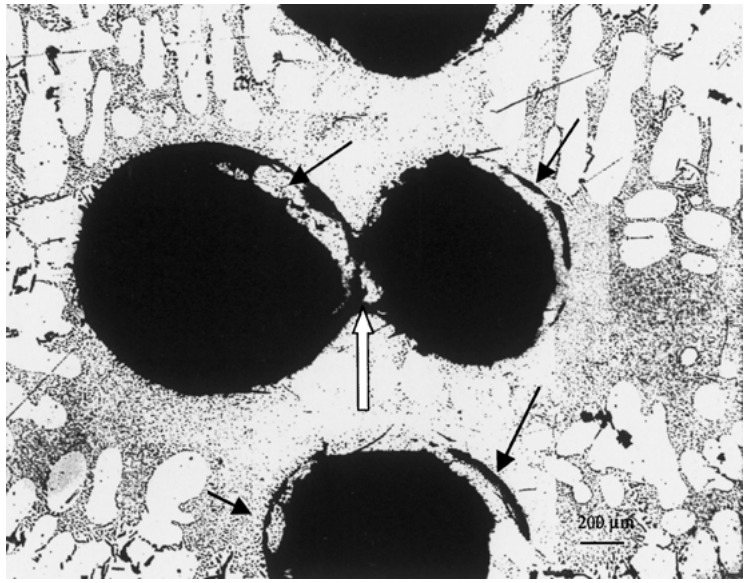

Figure 8 Optical micrograph obtained from Sr-modified Al-12%Si (A12SS) melt, cast after stirring. Arrows show solidifed alloy material entrapped within the oxide films. Open arrow shows how these oxide films can link two pores.

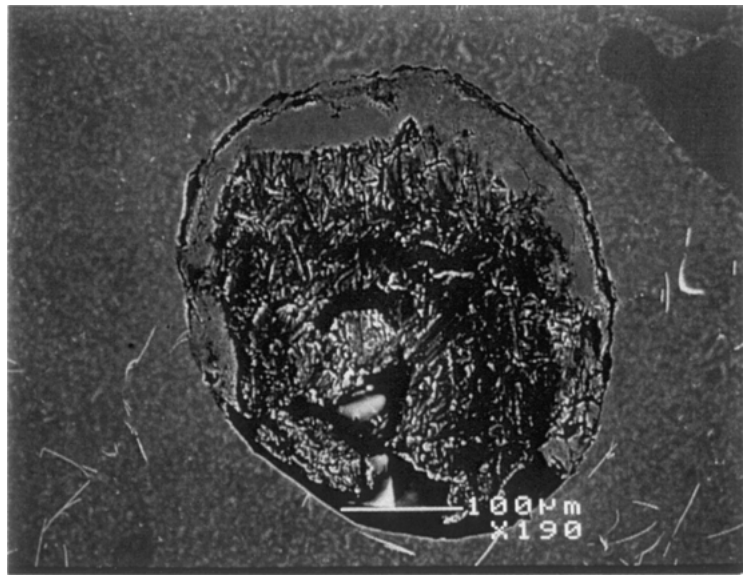

(a)

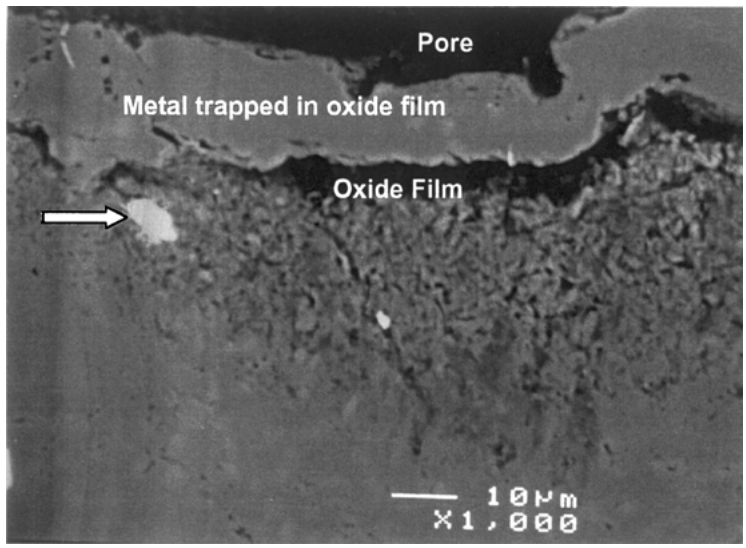

(b)

Figure 9 (a) SEM micrograph taken from the A12SS sample of Fig. 8, showing large size of the pore and eutectic Si region surrounding it, (b) high magnification micrograph of (a). Arrow in (b) points to an AlSrO particle.

in the pores displayed in Fig. 3 are also extremely shiny in nature.

To further confirm the relation of porosity to the presence of strontium oxide, some reduced pressure test (RPT) samples were also prepared. The samplings were taken from melts at 725°C, taking care to avoid any turbulence. The RPT or vacuum gas test is a simple qualitative test used widely in foundries to assess the hydrogen level in the melt prior to casting [21]. It consists essentially of solidifying a sample of the melt under reduced pressure (usually in the 50 to 100 mm Hg range). This encourages pore formation, the pores expanding due to the lowered pressure and providing a much more porous sample than under atmospheric conditions of solidification. The product, a cup-shaped specimen, permits the gas level to be assessed in three ways: (a) viewing the top of the sample and judging a puffed up surface as corresponding to a heavy gas content in comparison to a smooth or concave surface representing a low level; (b) sectioning the sample, examining the roughly polished surface for porosity and comparing with a photographic standard; and (c) finer polishing of the sectioned half to better observe the porosity profile through the use of sophisticated techniques [21, 22]. It has been shown that the results are influenced by the inclusions (including oxides) present in the melt [23], as these act as nucleating agents that facilitate bubble formation during solidification of the sample under reduced pressure.

In the present study, the sole purpose of introducing RPT samples was to facilitate examining the insides of the (enlarged) pores in the Sr-modified alloys. Fig. 4a displays a pore observed in Sr-modified 356 alloy, modified with 600 ppm Sr. A number of fine white particles

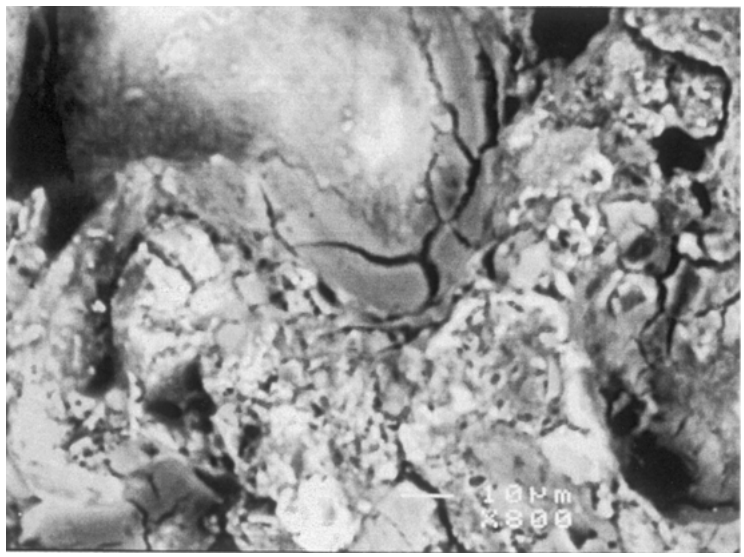

(a)

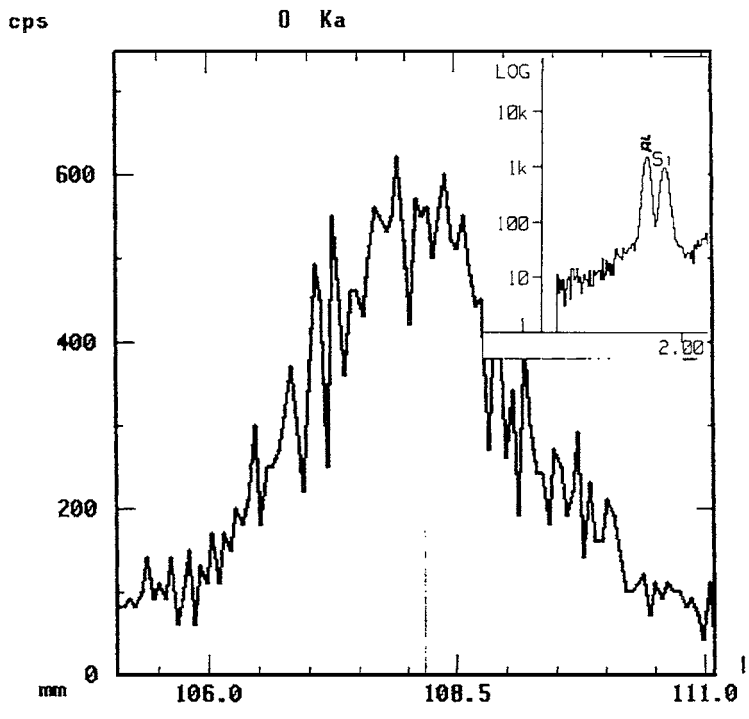

(b)

Figure 10 (a) SEM micrograph showing the bottom of an aluminum oxide-associated pore, and (b) composite of oxygen scan and EDX spectrum (inset) taken from (a).

are observed dotting the bottom of the pore (arrowed). The high magnification SEM micrograph in Fig. 4b reveals the size and distribution of these AlSrO particles. The Sr image taken from Fig. 4a is reproduced in Fig. 11c. The rounded morphology of the pore shown in Fig. 4a matches well with the observations of Laslaz and Laty [16] who noted that their oxide-contaminated melt samples displayed large, round pores, and in greater number. Correspondingly, the porosity levels would be larger, as well. The percentage porosity values in Table II for the Sr-modified alloys (containing Sr oxide inclusions) reflect this tendency.

A sampling taken from the same 600 ppm Sr-modified 356 alloy melt was used to conduct a Prefil (pressure filtration technique) test. The Prefil aparatus is one of the more recent techniques used to determine the melt cleanliness of aluminum foundry alloys (see, e.g., Simard *et al*. [24]). By passing ~2.5 kg of the molten metal through a filter under pressure (10 psi), the inclusions/films are concentrated in the region above the filter (pore sizes in the filter can vary from 0 to 123 μm). After the test, the solidified metal above the filter is sectioned, mounted and polished for metallographic examination. An example of the microstructure obtained from such a procedure is shown in Fig. 5. The arrows point to the formation of microporosity associated with the strontium oxide clusters. The wavelength dispersion spectroscopic (WDS) analysis confirmed the stoichiometric composition of this oxide to be $Al_{2.3}SrO_{3.3}$ (close to Al_2SrO_3).

Electron probe microanalysis was carried out for the same sample. Fig. 6 shows a series of micrographs depicting (a) the backscattered image, (b) the Al-, (c) the Sr-, and (d) the O images obtained from such AlSrO films that were associated with microporosity (arrowed in Fig. 6a).

The apparent stability of these oxides (since they were observed in a number of cases, examples of which were shown in the preceding figures) can be understood based on thermodynamic considerations, in terms of the oxidation potential of the elements (Sr and Al) involved [25]. Fig. 7 shows the plot of free energy of formation versus temperature for aluminum-, strontium-, and magnesium oxides (calculated per mole of oxygen). As can be seen, strontium oxide has a much higher negative free energy than aluminum oxide, so its formation can take place very easily during the melt treatment process when the Sr addition is made. The fact that the oxide

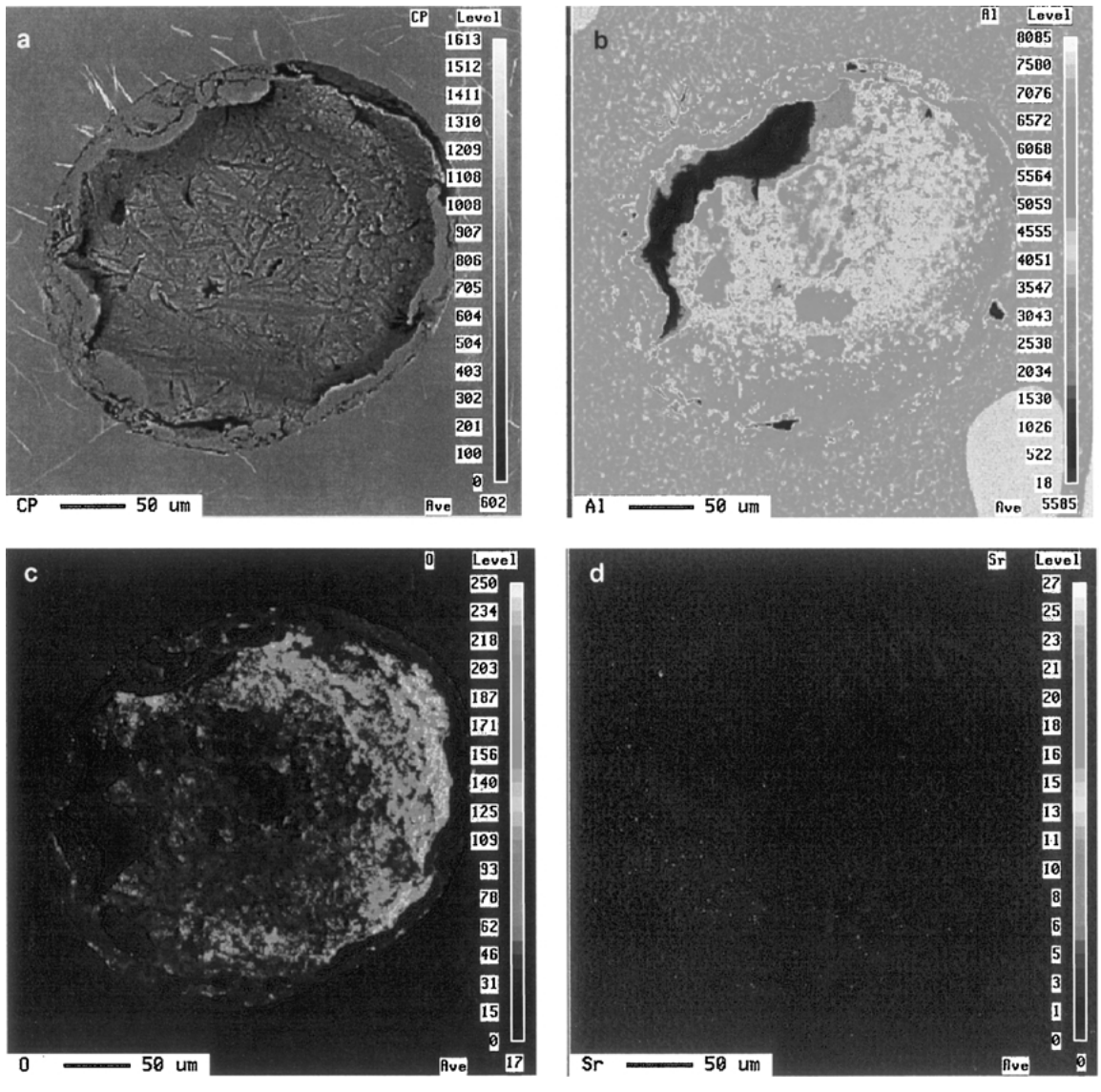

Figure 11 a) Backscattered image, and (b) the Al-, (c) O-, and (d) Sr images of an aluminum oxide-associated pore of the type shown in Fig. 8.

was often observed in the solidified microstructure in spite of degassing of the alloy melt (after the Sr addition and prior to casting) would suggest that the oxidation of the Sr in the melt took place during the 10 min-time interval when the melt was transferred from the larger to the 1-kg capacity crucible.

3.2. Role of aluminum oxide

To study the effect of aluminum oxides, in some cases, the melt was mechanically stirred to incorporate surface oxide films within the molten metal. The figures shown in this section were taken from samples that were obtained from such melt castings.

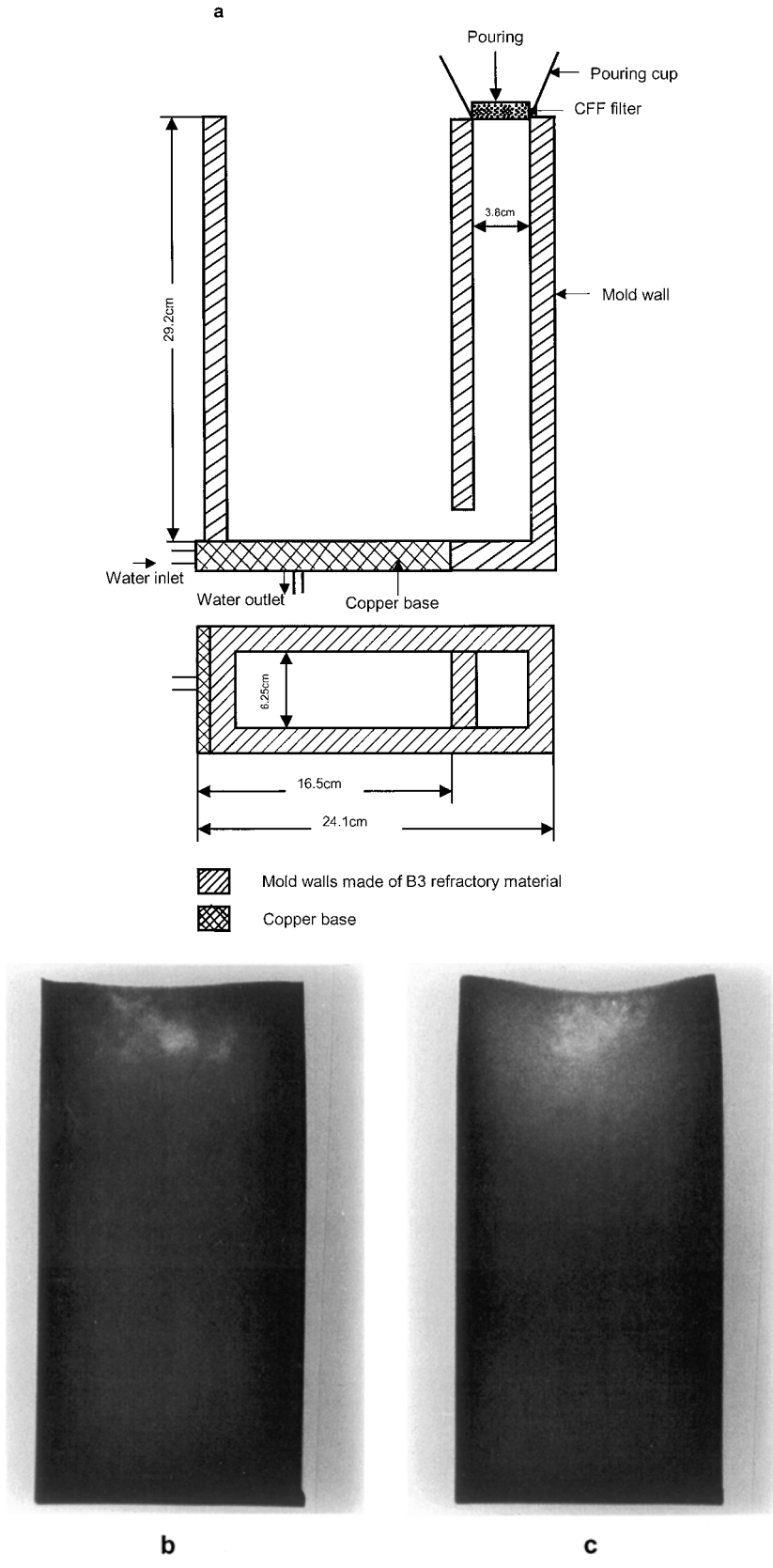

Figure 12 (a) Schematic diagram of end-chill mold and pouring arrangement for casting, (b,c) Radiographs of (b) H1T, and (c) H1S2 end-chill mold castings obtained from well-degassed melts of 319 alloy (H1: hydrogen level ~0.1 mL/100 g Al; T: grain refined melt; S2: 70 ppm Sr-modified melt).

Fig. 8 shows the optical micrograph obtained from the same Sr-modified Al-12%Si (Al2SS) melt, but cast after stirring. The arrows point to the presence of solidified alloy material within the pores, giving an indication that the molten metal was entrapped within the oxide films. The open arrow shows how two pores are linked together by means of such oxide films. Compared to the pores related to strontium oxide, aluminum oxide films lead to the formation of coarser and deeper pores (cf. Figs 2 and 8).

Fig. 9a is an SEM micrograph taken from the same sample. Two features are noted: the large size of the pore, and the eutectic Si phase surrounding the pore. A high magnification SEM micrograph of Fig. 9a reveals that the metal entrapped within the oxide film is separate from the edge of the pore, Fig. 9b. The "crumpled" region is probably part of the oxide film. The surrounding eutectic Si region is observed at the very bottom of the micrograph, and the white particle observed at the upper left corresponds to AlSrO (arrowed).

The spherical form of these pores suggests the entrapment of gases, particularly hydrogen (hydrogen being the most soluble), within their interiors. Given that, in the absence of inclusions, extremely high gas pressures are required to overcome the surface tension forces for the first hydrogen molecules to coalesce and form bubbles [20], this should most likely be true. Iwahori *et al*. [11] have also reported that in oxide-containing melts, the hydrogen content is not decreased after vacuum degassing.

The SEM micrograph of Fig. 10a shows the bottom of an aluminum oxide-associated pore. The crumpled nature of the aluminum oxide and the absence of the eutectic Si structure are evident. Fig. 10b shows a composite of an EDX and oxygen scan taken from this region. It is to be mentioned here that due to the depth of the pore, the oxygen profile was difficult to obtain. The Si peak in the EDX inset is thinner compared to that shown in Fig. 10c (taken from the strontium oxide-containing pore), where the Si and Sr peaks overlap. In this context, Huang *et al*. [20] have also commented upon the difficulty of identifying the size and morphology of these oxide films.

Fig. 11 shows the backscattered image and the Al-, O-, and Sr images of such a pore. The absence of visible microstructural Al-Si eutectic details within the pore are noted in Fig. 18a. The Al and O images, Fig. 11b and c, reveal clearly that the oxygen is concentrated within the pore, but is absent in the surrounding matrix, while the Al is concentrated in the matrix, but also to a reasonable extent within the pore, from which the presence of the aluminum oxide within the pore is confirmed. As for the Sr- image, Fig. 11d, the very tiny white spots (AlSrO or AlSiSr) observed indicate the presence of some impurity traces of the element probably trapped within the oxide film.

From the above observations, it may be suggested that the entrapped Al_2O_3 oxide films are very effective in creating porosity. Degassing (using an inert gas such as pure, dry argon injected by means of a graphite rotary impeller running at high (200 rpm) speed) can be employed to remove the Al_2O_3 films or particles. In the case of Sr-modified alloys, however, due to the high stability of the AlSrO oxides, filtration using fine ceramic foam filters (20 ppi or 20 pores per inch) is recommended to prevent their passage into the final casting.

In keeping with these recommendations, a series of castings were prepared from 319 alloy using an end-chill mold, and used in an extensive investigation to study the effect of microstructure on the alloy performance [26, 27]. A schematic diagram of the mold is shown in Fig. 12a. The inner surfaces of the mold were covered with 2 mm thick steel plates to prevent moisture from penetrating into the casting. The mold was dried by preheating at 120°C for 3 hours, before the melt was poured through the pouring cup which had a ceramic foam filter (20 ppi) fitted to its bottom to remove oxides and other inclusions from entering the mold.

An example of the quality of castings obtained using these procedures is displayed in Figs 12b and c, which show the radiographs of two end-chill mold castings that were obtained from well-degassed 319 alloy melts (hydrogen level ~0.1 mL/100 g Al), the left one corresponding to a grain refined melt (0.02 wt% Ti content), and the right one obtained from a 70 ppm Sr-modified melt. Note the absence of clustered pores in either case. Both castings exhibited light porosity (rated 1-2 according to ASTM 155 testing standards), indicating the effectiveness of this technique in removing most of the Al_2O_3 and AlSrO oxides, providing sound castings and, hence, acceptable performance in terms of mechanical properties.

4. Conclusions

An extensive investigation was carried out to study the role of strontium and aluminum oxides in relation to porosity formation in Al-Si casting alloys, using experimental and industrial Al-Si alloys, modified with Sr (up to 600 ppm). Metallographic samples obtained from different techniques (thermal analysis, reduced pressure tests and the Prefil technique) were analyzed using optical and scanning electron microscopy, image analysis, as well as EDX, WDS and EPMA analyses. Based on the results obtained, the following could be concluded.

1. Pores observed in Sr-modified alloys are frequently associated with strontium oxides (films or particles). These particles/films are formed during melting, due to the high oxygen affinity of strontium, and are extremely difficult to be removed during degassing (using pure argon and a rotary impeller). The stoichiometric composition of these oxides is found to be $Al_{2.3}SrO_{3.3}$ (or Al_2SrO_3) from WDS analysis.

2. The morphology of the pores (round or irregular) is determined by the form of oxide, i.e., fine, dispersed particles or thick films. The rounded pores are also observed surrounded by Al-Si eutectic regions.

3. Aluminum oxide films trapped in the molten metal can lead to the formation of coarser and deeper pores than those formed due to strontium oxide. These pores can also link with each other through the oxide films. Such pores are characterized by the presence

of solidified metal trapped within the aluminum oxide films, close to the periphery, with no Al-Si eutectic features observed within the pore. The form of these pores is controlled by the amount of gases entrapped within the pores during solidification. Correspondingly, the porosity level is also increased.

4. The aluminum and strontium oxides also act as favorable sites for the precipitation of other microstructural constituents, such as the β-Al_5FeSi iron intermetallic phase.

Acknowledgements

Financial and in-kind support received from the Natural Sciences and Engineering Research Council of Canada (NSERC), the Centre québécois de recherche et de développement de l'aluminium (CQRDA), the Fondation de l'Université du Québec à Chicoutimi (FUQAC), General Motors Powertrain Group (U.S.A.), Corporativo Nemak (Mexico) and ABB Bomem Inc. (Quebec) is gratefully acknowledged. The authors would also like to thank Mr. Glenn Poirier of the Microanalysis Laboratory, Earth and Planetary Sciences, McGill University for carrying out the SEM/EDX, EPMA and WDS analyses.

References

1. D. ARGO and J. E. GRUZLESKI, *AFS Trans.* **96** (1988) 65.
2. P. D. LEE and S. SRIDHAR, *Int. J. Cast Metals Res.* **13** (2000) 185.
3. R. FUOCO, E. R. CORREA and H. GOLDENSTEIN, *AFS Trans.* **104** (1996) 1151.
4. S. D. McDONALD, K. NOGITA, A. K. DAHLE, J. A. TAYLOR and D. H. St. JOHN, *ibid.* **108** (2000) 463.
5. J. R. DENTON and J. A. SPITTLE, *Mater. Science Technol.* **1** (1985) 305.
6. B. KOLTE, *Modern Casting* **75**(5) (1985) 33.
7. H. SHAHINI, *Scand. J. Metallurgy* **14** (1985) 306.
8. G. K. SIGWORTH, *AFS Trans.* **91** (1983) 7.
9. J. M. KIM, H. W. KWON and C. R. LOPER JR., *AFS Trans.* **104** (1996) 743.
10. A. K. DAHLE, J. HJELEN and L. ARNBERG, in Proc. 4th Decennial Int. Conf. on "Solidification Processing 1997," University of Sheffield, Sheffield, UK, 1997.
11. H. IWAHORI, K. YONEKURA, Y. YAMAMOTO and M. NAKAMURA, *Imono (Journal of Japan Foundrymen's Society)* **61**(1) (1989) 31.
12. H. IWAHORI, K. YONEKURA, Y. YAMAMOTO and M. NAKAMURA, *AFS Trans.* **98** (1990) 167.
13. S. JACOB, M. GARAT, G. LASLAZ, P. MEYER, P. GUERIN and R. ADAM, *Hommes et Fonderie* **258** (1995) 45.
14. X. CAO and J. CAMPBELL, *AFS Trans.* **108** (2000) 391.
15. R. FUOCO, E. R. CORREA and M. DE ANDRADE BASTOS, *ibid.* **109** (2001) 403.
16. G. LASLAZ and P. LATY, *ibid.* **99** (1991) 83.
17. Q. T. FANG and D. A. GRANGER, *ibid.* **97** (1989) 989.
18. A. M. SAMUEL, F. H. SAMUEL, H. W. DOTY and S. VALTIERRA, *ibid.* **109** (2001) Paper 01-170, 679–696.
19. F. H. SAMUEL, P. OUELLET and A. SIMARD, *Int. J. Cast Metals Res.* **12** (1999) 49.
20. L. W. HUANG, W.-J. SHU and T.-S. SHIH *AFS Trans.* **108** (2000) 547.
21. S. K. DeWEESE, R. ATKINSON and W. RASMUSSEN, *Modern Casting* **82**(4) (1992) 29–31.
22. A. M. SAMUEL and F. H. SAMUEL, *Metall. Trans. A* **24A** (1993) 1857.
23. K. J. BRONDYKE and P. D. HESS, *Trans. AIME* **230** (1964) 1542.
24. A. SIMARD, J. PROULX, D. PAQUIN, F. H. SAMUEL and N. HABIBI, in "Proc. 6th AFS International Conference on Molten Aluminum Processing," Orlando, Florida, U.S.A., November 11–13, 2001, 92–113.
25. W. M. LATIMER, "The Oxidation States of the Elements and Their Potentials in Aqueous Solutions," 2nd ed. (Prentice-Hall, Inc., Englewood Cliffs, N.J., 1952) pp. 280–283, 315–323.
26. A. M. SAMUEL and F. H. SAMUEL, *J. Mater. Sci.* **30** (1995) 4823.
27. Z. MA, Ph.D. Thesis, Université du Québec à Chicoutimi, Chicoutimi, Canada (Unpublished results, 2000).

Received 18 March
and accepted 25 November 2002